Journal of Materials Chemistry

Cite this: *J. Mater. Chem.*, 2011, **21**, 11177

www.rsc.org/materials

PAPER

Synthesis, characterization and photophysical properties of polyfunctional phenylsilsesquioxanes: $[o\text{-RPhSiO}_{1.5}]_8$, $[2,5\text{-R}_2\text{PhSiO}_{1.5}]_8$, and $[\text{R}_3\text{PhSiO}_{1.5}]_8$. compounds with the highest number of functional units/unit volume†

Santy Sulaiman,[b] Jin Zhang,[b] Theodore Goodson, III[bc] and Richard M. Laine*[ab]

Received 19th April 2011, Accepted 26th May 2011
DOI: 10.1039/c1jm11701g

The availability of pure samples of *o*-Br_8OPS, 2,5-Br_{16}OPS, and Br_{24}OPS provides a rare opportunity to synthesize sets of corresponding stilbene derivatives: *o*-$RStyr_8$OPS, $RStyr_{16}$OPS, and $RStyr_{24}$OPS where R = 4-methyl (Me), Boc-protected 4-amino (NBoc), or 4-acetoxy (Ace). These derivatives show unique UV-Vis absorption and photoluminescent behavior that points to interesting interactions between the organic tethers and the silsesquioxane cage. *o*-$RStyr_8$OPS shows blue-shifts in the absorption spectra compared to *p*-$MeStyr_8$OPS, suggesting that the stilbene groups sit over and interact with the face of the electrophilic silsesquioxane cage as is the case with the parent molecule, *o*-Br_8OPS. The emission spectra of *o*-$RStyr_8$OPS are similar to *p*-$MeStyr_8$OPS indicating similar excited states involving the core LUMO. $RStyr_{16}$OPS exhibits absorption and emission spectra as well as Φ_{PL} similar to 1,4-distyrylbenzene, pointing to disruption in conjugation with the silsesquioxane cage because of steric interactions. $RStyr_{24}$OPS offers absorption maxima that are blue-shifted and emission maxima that are red-shifted relative to $RStyr_{16}$OPS. We speculate that $RStyr_{24}$OPS is so sterically hindered that interactions with the cage face must occur. NBoc$Styr_{24}$OPS and Ace$Styr_{24}$OPS show moderate Φ_{PL} and high two photon cross-section values, leading us to conclude that there are two excited states of nearly equivalent energy in these molecules with similar decay rates: a normal radiative π–π^* transition and charge transfer involving the silsesquioxane cage. These same functional groups can be anticipated to offer much greater two photon absorption if different methods can be found for protecting the free amine from oxidation or replacing the acetoxy group (*e.g.* perhaps using alkyl or aryl groups).

Introduction

In the past few years, we and others have sought to use the 3-D nature of functionalized silsesquioxanes (SQs)[1–3] to develop novel hybrid organic/inorganic components for electronic and photonic devices.[2,4–12] The rationale for this effort comes from the fact that the T_8 and Q_8 derivatives, see Fig. 1, place functional groups in each octant in Cartesian space providing good-to-excellent solubility allowing facile purification. Furthermore, the central cage provides the heat capacity of silica often improving thermal stabilities up to 100 °C higher compared to all-organic compounds with structures similar to SQs or its organic tethers[13–15] or model compounds such as organic triethoxysilanes. In addition, these compounds are easily made in 0.1–1 kg quantities in short periods of time.[16,17]

Perhaps most importantly, recent work indicates that the cage is not an innocuous insulating component but rather appears to offer 3-D conjugation in the excited state promising novel semiconductor properties.[10,11] In the latter case we have shown that the pure methyl-stilbene SQs, $[o\text{-MeStyrPhSiO}_{1.5}]_8$ (*o*-$MeStyr_8$OPS) and $[p\text{-MeStyrPhSiO}_{1.5}]_8$ (*p*-$MeStyr_8$OPS), show red-shifts in their emission behavior of up to 80 nm relative to molecular *trans*-stilbene as seen in Fig. 2.[11]

Furthermore, we also find that the two photon absorption cross-sections (TPA) per moiety of methoxy- and amino-vinylstilbene SQs, $[p\text{-MeOStilCH} = \text{CHSiO}_{1.5}]_8$ and $[p\text{-NH}_2\text{StilCH} = \text{CHSiO}_{1.5}]_8$, are quite high relative to model compounds (see Table 1). In these instances, the observed behaviors can be directly correlated with the formation of charge transfer (CT)

[a]*Materials Science and Engineering, University of Michigan, 2300 Hayward St, Ann Arbor, USA. E-mail: talsdad@umich.edu; Fax: +01 734-7634788; Tel: +01 734-7646203*
[b]*Macromolecular Science and Engineering, University of Michigan, 2300 Hayward St, Ann Arbor, USA. E-mail: talsdad@umich.edu; Fax: +01 734-7634788; Tel: +01 734-7646203*
[c]*Dept of Chemistry, University of Michigan, 930 N. University, Ann Arbor, MI, 48109-1055. E-mail: tgoodson@umich.edu*
† Electronic Supplementary Information (ESI) available: Spectroscopic data for compounds synthesized. See DOI: 10.1039/c1jm11701g/

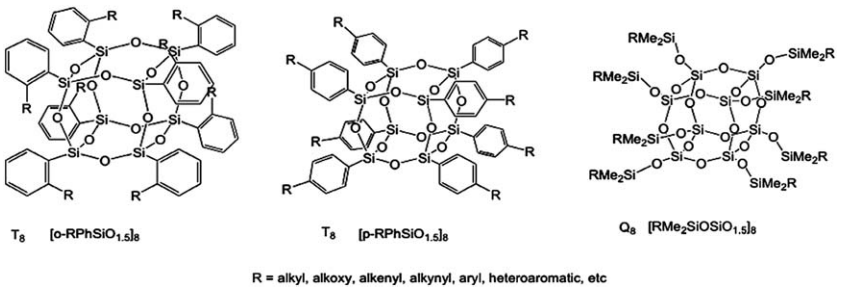

Fig. 1 3-D symmetrical T_8 and Q_8 compounds.

excited states wherein the peripheral MeO- and NH_2 groups donate electron density to the cage in the excited state as supported by solvatochromism studies.[10,11]

These results coupled with our recent discovery of methods of making very pure [*o*-$BrPhSiO_{1.5}]_8$, [2,5-$Br_2PhSiO_{1.5}]_8$, [$Br_3PhSiO_{1.5}]_8$, provided the impetus to explore the functionalization of these compounds.[18] In principle, these brominated [$PhSiO_{1.5}]_8$ or OPS (octaphenylsilsesquioxane) derivatives offer the potential to introduce 8, 16 or $\approx$ 24 functional groups in the same volume. Furthermore, these functional groups are expected to offer extended conjugation *via* the central phenyl ring and through the center of the cage. Also of potential interest is the fact that the molecules synthesized here have some of the highest densities of functional groups per unit volume possible. Assuming spherical shapes, these polyfunctional SQs have diameters of approximately 1.5 nm.[19] In contrast, for example, PAMAM dendrimers[20] with comparable numbers of functional groups (see Table 2) obtained only at much greater diameters and only as surface functional groups.

We have chosen functional groups per unit volume of individual molecules and compared them to dendrimers as opposed to total densities of molecules per cc. In our crystal structures,[19] we do not see interdigitation; thus, these values are realistic at all length scales.

The extended conjugation in each functional group coupled with the potential for 3-D conjugation, considerable charge transfer behavior and the fact that in earlier studies we saw exceptional two-photon absorption cross-sections suggest possible applications in optical limiting and enhanced solar energy harvesting. As we report below, the results of these studies provide unexpected properties that may be useful for these applications.

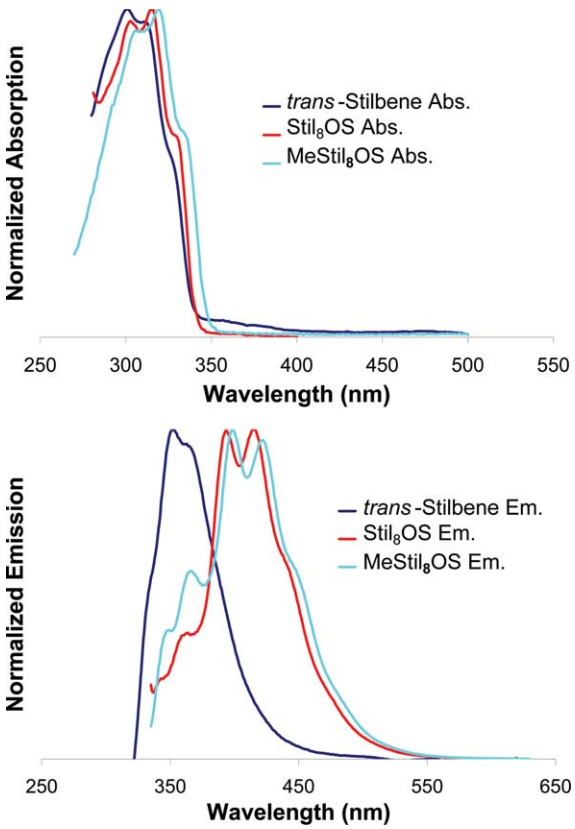

Fig. 2 UV-Vis absorption and PL emission of *trans*-stilbene and [*p*-Me(H)StyrPh$SiO_{1.5}]_8$ in THF.[11]

Experimental section

Synthetic methods

Materials. Dichloromethane (CH_2Cl_2) was purchased from Fisher Scientific and distilled from CaH_2 under N_2 prior to use. Dioxane and THF were purchased from Fisher Scientific and

Table 1 TPA properties of SQ derivatives.[10,11]

Sample	δ (GM)	δ/moiety (GM)	λ_{max} nm
[*p*-MeStil$SiO_{1.5}]_8$	11	1.2	735
[*p*-Me_2NStil$SiO_{1.5}]_8$	211	26	755
[StilCH = $CHSiO_{1.5}]_8$	25	3	705
[*p*-MeOStilCH = $CHSiO_{1.5}]_8$	110	14	705
[*p*-NH_2StilCH = $CHSiO_{1.5}]_8$	810	101	720

Table 2 Physical characteristics of PAMAM dendrimers.[20]

Generation	No. of surface groups	Molecular weight[a]	Diameter (nm)[b]
0	4	517	1.5
1	8	1430	2.2
2	16	3256	2.9
3	32	6909	3.6

[a] Molecular weight is based on defect-free, ideal-structure, amine-terminated dendrimers. [b] Molecular dimensions determined by size-exclusion chromatography.

distilled from Na/benzophenone under N_2 prior to use. [*o*-$BrPhSiO_{1.5}$]$_8$ (*o*-Br_8OPS), [2,5-$Br_2PhSiO_{1.5}$]$_8$ (Br_{16}OPS), and [$Br_3PhSiO_{1.5}$]$_8$ (Br_{24}OPS) were synthesized using previously reported methods.[18] All other chemicals were purchased from Sigma-Aldrich, Fisher Scientific, or Strem Chemicals, Inc., and used as received.

Synthesis of 4-NBocStyrene. To a dry 50-mL Schlenk flask under N_2 was added a solution of 2.0 g (12 mmol) di-*tert*-butyl-dicarbonate in 10 mL THF, followed by a solution of 1.2 g (10 mmol) 4-vinylaniline in 10 mL THF. The mixture was then refluxed for 24 h. After cooling to room temperature, the reaction mixture was partitioned between 25 mL of DI H_2O and 25 mL of CH_2Cl_2. The layers were separated and the aqueous layer was washed twice with 25 mL of CH_2Cl_2. The organic layer was then washed with 25 mL of DI H_2O, dried over Na_2SO_4, and concentrated to give a yellow residue, which was further purified to by column chromatography on silica eluting with hexane/ethyl acetate (70 : 30) to give the product as white waxy solid.

General Heck reaction of *o*-Br_8OPS. To a dry 10-mL Schlenk flask under N_2 was added 0.50 g (0.3 mmol, 2.4 mmol-Br) of *o*-Br_8OPS, 22 mg (0.046 mmol) of Pd[P(*t*-Bu_3)]$_2$, and 21 mg (0.023 mmol) of $Pd_2(dba)_3$. 1,4-dioxane (3 ml) was then added by syringe, followed by NCy_2Me (3.7mmol, 0.8 ml) and R-styrene (8.70 mmol). The mixture was stirred at 70 °C for 24 h and then quenched by filtering through 1 cm Celite, which was washed with 5 ml THF. The solution was then precipitated into 200 ml methanol, filtered, and the solid re-dissolved in 10 ml THF. This solution was then filtered again through a 1 cm Celite column to remove any remaining Pd particles, and re-precipitated into 200 ml methanol. Analytical data are presented in the discussion section below.

General Heck reaction of Br_{16}OPS. To a dry 10-mL Schlenk flask under N_2 was added 0.50 g (0.22 mmol, 3.5 mmol-Br) of 2,5-Br_{16}OPS, 22 mg (0.046 mmol) of Pd[P(*t*-Bu_3)]$_2$, and 21 mg (0.023 mmol) of $Pd_2(dba)_3$. 1,4-dioxane (5 ml) was then added by syringe, followed by NCy_2Me (5.6 mmol, 1.2 ml) and R-styrene (10.5 mmol). The mixture was stirred at 70 °C for 24 h and then quenched by filtering through 1 cm Celite, which was washed with 5 ml THF. The solution was then precipitated into 200 ml methanol, filtered, and the solid re-dissolved in 10 ml THF. This solution was then filtered again through a 1 cm Celite column to remove any remaining Pd particles, and re-precipitated into 200 ml methanol. The product is further purified by column chromatography. Analytical data are presented in the discussion section below.

General Heck reaction of Br_{24}OPS. To a dry 10-mL Schlenk flask under N_2 was added 0.50 g (0.17 mmol, 3.9 mmol-Br) of Br_{24}OPS, 22 mg (0.046 mmol) of Pd[P(*t*-Bu_3)]$_2$, and 21 mg (0.023 mmol) of $Pd_2(dba)_3$. 1,4-dioxane (3 ml) was then added by syringe, followed by NCy_2Me (6.2 mmol, 1.32 ml) and R-styrene (12 mmol). The mixture was stirred at 70 °C for 24 h and then quenched by filtering through 1 cm Celite, which was washed with 5 ml THF. The solution was then precipitated into 200 ml methanol, filtered, and the solid re-dissolved in 10 ml THF. This solution was then filtered again through a 1 cm Celite column to remove any remaining Pd particles, and re-precipitated into 200 ml methanol. The product is further purified by column chromatography. Analytical data are presented in the discussion section below.

Removal of residual Pd catalyst. To a dry 50-mL Schlenk flask under N_2 was added 1.0 g of RStyr$_x$OPS dissolved in 10 mL of toluene and 0.1 g of *N*-acetyl-L-cysteine dissolved in 1 mL of THF. The solution was stirred overnight at room temperature and then filtered through a short silica gel column to remove the insoluble Pd-cysteine complex. The filtrate was then concentrated by rotary evaporation and precipitated into 200 mL of methanol or hexane. The product was filtered and dried in vacuo overnight.

Deprotection of NBocStyr$_x$OPS. To a dry vial under N_2 was added 10 mg of NBocStyr$_x$OPS dissolved in 1 mL of THF and 1 mL of 37% HCl solution. The reaction was stirred overnight at room temperature. The reaction was then neutralized with saturated $NaHCO_3$ solution and extracted with CH_2Cl_2 (3 × 10 mL). The combined organic layer was washed with DI H_2O (3 × 10 mL), dried over Na_2SO_4, and the solvent evaporated in vacuo to give light brown solid as product. Analytical data are provided in the results section.

Analytical methods

Gel permeation chromatography. GPC analyses were done on a Waters 440 system equipped with Waters Styragel columns (7.8 × 300, HT 0.5, 2, 3, 4) with RI detection using Waters refractometer and THF as solvent. The system was calibrated using polystyrene standards and toluene as reference.

Thermogravimetric analyses. TGAs were run on a SDT Q600 Simultaneous Differential DTA-TGA Instrument (TA Instruments, Inc., New Castle, DE). Samples (15–25 mg) were loaded in alumina pans and ramped at 10 °C min^{-1} to 1000 °C under dry air with a flow rate of 60 mL/min.

Matrix-assisted laser desorption/time-of-flight spectrometry. MALDI-TOF was done on a Micromass TofSpec-2E equipped with a 337 nm nitrogen laser in positive-ion reflectron mode using poly(ethylene glycol) as calibration standard, dithranol as matrix, and $AgNO_3$ as ion source. Samples were prepared by mixing solutions of 5 parts matrix (10 mg mL^{-1} in THF), 5 parts sample (1 mg mL^{-1} in THF), and 1 part $AgNO_3$ (2.5 mg mL^{-1} in water) and blotting the mixture on target plate.

UV-Vis spectrometry. UV-Vis spectra were taken on a Shimadzu UV-1601 UV-Vis transmission spectrometer in CH_2Cl_2. Samples were dissolved in CH_2Cl_2 and diluted to a concentration (10^{-3}-10^{-4} M) where the absorption maximum was less than 10% for a 1 cm path length.

Photoluminescence spectrometry. Photoluminescent spectra were taken on a Fluoromax-2 fluorimeter in THF. Samples from UV-VIS spectroscopy were diluted (10^{-5} to 10^{-7} M) to avoid excimer formation and fluorimeter detector saturation.

Two photon studies

Steady state measurements. All compounds were dissolved in CH_2Cl_2 (Sigma-Aldrich, spectrophotometric grade) for carrying out the optical measurements. The absorption spectra of the molecules were measured using an Agilent (Model No. 8341) spectrophotometer. In order to measure the molar extinction coefficients, the original stock solutions were diluted to 10^{-6} M. The fluorescence spectra were acquired using a Spex-fluorolog spectrofluorimeter. The quantum yields of the molecules were measured using a known procedure.[21] Bis-MSB [*p*-bis(*o*-methylstyryl)benzene] has been used as the standard. The absorbance was limited to less than 0.03. The solutions were purged with argon for 3 min prior to measuring their emission spectra. Then, the following relation was used to measure the quantum yield:[21]

$$\phi_F = (\phi_F)_S \frac{\int J(\bar{\nu})d\bar{\nu}}{\int J_S(\bar{\nu})d\bar{\nu}} \frac{(J_a)_S}{J_a} \frac{n^2}{n_S^2}$$

where,

$(\phi_F)_S$ = Quantum yield of the standard

$\int J(\bar{\nu})d\bar{\nu}$ = Area under the fluorescence emission curve for the sample

$\int J_S(\bar{\nu})d\bar{\nu}$ = Area under the fluorescence emission curve for the standard.

$(J_a)_S$ = Absorbance of the standard

J_a = Absorbance of the sample

n^2 = Refractive index of the solvent used for the sample.

$n^2{}_s$ = Refractive index of the solvent used for the standard.

Two-photon excited fluorescence measurements. In order to measure the two photon absorption cross sections, we followed the two photon excited fluorescence (TPEF) method.[22] A 10^{-4} M Coumarin 307 (7-ethylamino-6-methyl-4-trifluoro-methylcoumarin) solution in methanol was used as the reference for measuring TPA cross-sections at different wavelengths. The laser used for the study was a Mai Tai Diode-pumped Mode-Locked Ti:sapphire laser, which is tunable from 700 to 1000 nm. The beam was directed on to the sample cell (quartz cuvette, 0.5 cm path length) and the resultant fluorescence was collected in a direction perpendicular to the incident beam. A 1″ focal length plano-convex lens was used to direct the collected fluorescence into a monochromator. The output from the monochromator was coupled to a PMT. The photons were converted into counts by a photon counting unit. A logarithmic plot between collected fluorescence photons and input intensity gave a slope of two, ensuring a quadratic dependence. The intercept enabled us to calculate the two photon absorption cross sections at different wavelengths.

Results and discussion

In previous studies, we used Heck coupling as a means to introduce a variety of functional groups to brominated- (reaction 1) and iodinated- (reaction 2) OPS.[17,23] In these studies, we had not as yet learned to control bromination selectivity and opted for compounds with less than eight bromines to minimize the potential for double substitution at a single phenyl group. Even so, double bromination was still observed at 3–5% of the total bromine incorporated. This was the motivation for moving to the iodination studies where double iodination was not observed. With our recent discovery of routes to pure *o*-Br_8OPS, Br_{16}OPS, and Br_{24}OPS,[18] we can now extend our studies to making sets of octa-, hexadeca- and tetraicosa-styrenyl substituted OPS compounds. The motivation, as noted above, is to extend our knowledge concerning the cage-moiety interactions as it affects photophysical properties. Scheme 1 shows the general reaction schemes explored.

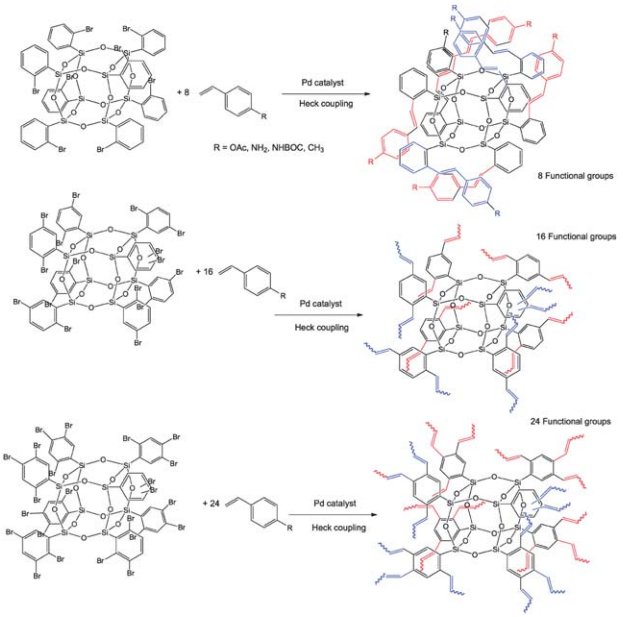

Scheme 1 Heck coupling studies on *o*-Br_8OPS, 2,5-Br_{16}OPS and Br_{24}OPS. Preparation of selected functionalized StyreneOPS for comparison of photophysical properties.[18]

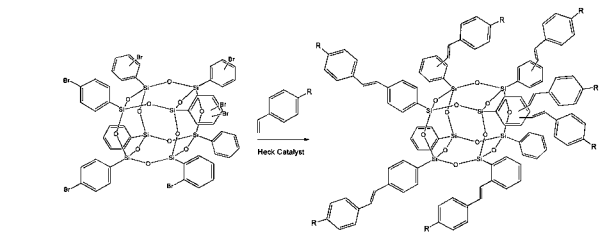

(1)

23

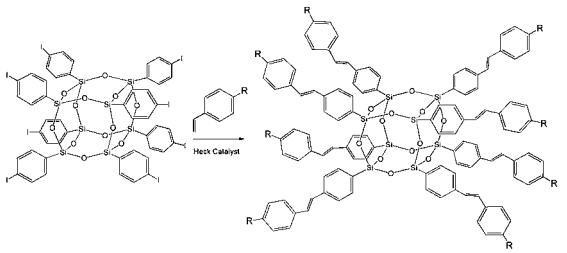

(2)

We begin with a discussion of our synthetic methods as a prelude to discussing characterization and thereafter photophysical properties for a set of three different StyreneOPS systems: the *para*-methyl, -acetoxy and Boc-protected amine.

Synthesis methods

Heck coupling at the *ortho* position is relatively slow because of steric interactions, see reaction (3) and Fig. 3. As a consequence, most reactions were run at 70 °C/24 h, in contrast to our earlier studies where the reactions were run at room temperature (48 h).[11,12] Tables 6–8 list general characterization data for the compounds prepared. In general, purities were quite high as witnessed by the ceramic yields, which are close to those calculated, Tables 7, 8. Table 8 provides data for NBocStyr$_x$OPS separately as the analyses need some explanation.

Heck coupling reactions between crystalline Br$_x$OPS (x = 8, 16, 24) and the target *p*-RStyrene were run under much more rigorous conditions compared to our previous work using BrStyrenylOS.[10,23] The close proximity of the *ortho*-Br groups to the SQ core presents a challenge in obtaining complete conversion to the Heck coupling product. This was achieved using higher concentrations of *p*-RStyrene and elevated temperatures.

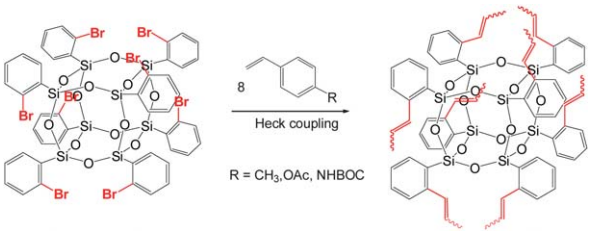

(3)

As noted above, we chose three different R groups in this work. The simplest methyl derivatives are used for comparison with the small molecule analog and as a baseline for the other derivatives. NH_2VinylStilbeneOS previously synthesized from *p*-BrStyrenylOS shows CT behavior in solution, and we would like to investigate how this phenomenon is affected by increases in the number of chromophores in the NH_2Stry$_x$OPS systems. However, due to the basic nature of $-NH_2$ groups and the instability of SQ cages in base, –Boc protection was used to prevent unwanted degradation during synthesis. Deprotection was possible for the octa-*ortho*-compound but the higher functionality congeners were found to oxidize rapidly during deprotection and thus photophysical properties were measured for the NBoc derivatives. The acetoxy- group was chosen as it can be hydrolyzed to give hydroxyl- groups, which can be used as a starting point for further functionalization to make supramolecular or 3-D nanoarchitectures.

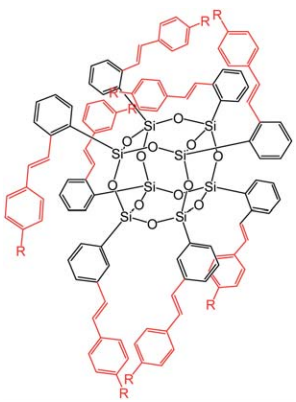

Fig. 3 *o*-RStyr$_x$OPS bond lengths and angles exaggerated for clarity.

It is well-known that SQ cages have high affinity for the transition metals commonly used as catalyst in coupling reactions, such as palladium and ruthenium.[24] The Heck coupling products of Br$_x$OPS still contain residual palladium catalyst, even after several precipitation steps, as evidenced by the grayish tint of the products. Further removal of residual palladium was achieved by treating the crude products with the well-known palladium complexing additive *N*-acetyl-L-cysteine.[25] The palladium-cysteine complex is soluble in polar solvents such as THF and methanol, but highly insoluble in non-polar solvents such as toluene. Therefore, the palladium-cysteine complex can be removed either during filtration of the original reaction mixture, as it precipitated out of toluene, or during the precipitation as it goes into solution in methanol.

The Heck coupling reactions of Br$_x$OPS produced some unwanted byproducts, which according to the GPC analyses are most likely dimeric in nature (*i.e.* two SQ molecules bridged by an organic tether). These byproducts were not observed in our earlier work with BrStyrenylOS.[10] We believe that dimer formation arises because of the harsher reaction conditions used in this set of experiments, especially the high concentration of reagents in the reaction mixture. The byproducts were removed either by column chromatography or selective precipitation to give pure products per GPC analyses.

Solubilities

All of the synthesized compounds are soluble in moderately polar organic solvents such as THF, 1,4-dioxane, CH_2Cl_2, and $CHCl_3$. MeStyr$_x$OPS and AceStyr$_x$OPS are insoluble in highly polar solvents such as methanol, and in nonpolar solvents such as hexane. NBocStyr$_x$OPS are soluble in methanol, and were therefore purified by precipitation into hexane.

Molecular characterization

MALDI-ToF spectra of RStyr$_x$OPS are shown in Figures S1-S6. It should be noted that although the compounds synthesized in this work are labeled as having 8, 16, or 24 groups per molecule, those numbers reflect an average of the actual number of functional groups present per molecule. The starting materials used in this work (*o*-Br$_8$OPS, Br$_{16}$OPS, and Br$_{24}$OPS) were purified by multiple recrystallization; however, MALDI-ToF spectra of these materials still show small amounts of other brominated species (*e.g.* Br$_7$OPS, Br$_{15}$OPS, Br$_{22}$OPS, *etc.*) present in the system.[18]

Tables 3–5 detail the different molecular species present in RStyr$_x$OPS and their percentages based on MALDI-ToF data. Even though each set of compounds (*o*-RStyr$_8$OPS, RStyr$_{16}$OPS, and RStyr$_{24}$OPS) was synthesized using starting material from the same batch, their MALDI-ToF data show different compositions of molecular species. For example, MALDI-ToF data for *o*-MeStyr$_8$OPS and *o*-AceStyr$_8$OS show different percentages for the 7-mer and the 8-mer, and *o*-NH_2Styr$_8$OS show the presence of the 9-mer, which is not present in the other two compounds. We attribute these results to differences in ionization potentials of the compounds rather than substitutional variations.

Table 3 Molecular species present in $MeStyr_xOPS$

o-$MeStyr_8OPS$		$MeStyr_{16}OPS$		$MeStyr_{24}OPS$	
Species	%	Species	%	Species	%
o-$MeStyr_7OPS$	5	$MeStyr_{14}OPS$	2.4	$MeStyr_{22}OPS$	18.5
o-$MeStyr_8OPS$	95	$MeStyr_{15}OPS$	30.5	$MeStyr_{22}BrPh_1OPS$	5.1
		$MeStyr_{16}OPS$	62.2	$MeStyr_{23}OPS$	47.0
		$MeStyr_{17}OPS$	4.9	$MeStyr_{23}BrOPS$	5.8
Average: 7.95		Average: 15.7		$MeStyrenyl_{24}OPS$	23.6

Table 4 Molecular species present in NH_2Styr_xOPS

o-NH_2Styr_8OPS		$NH_2Styr_{16}OPS$	
Species	%	Species	%
o-NH_2Styr_8OPS	89.6	$NH_2Styr_{16}OPS$	100
o-NH_2Styr_9OPS	10.4		
Average: 8.1		Average: 16.0	

Table 5 Molecular species present in $AceStyr_xOPS$

o-$AceStyr_8OPS$		$AceStyr_{16}OPS$	
Species	%	Species	%
o-$AceStyr_7OPS$	23.6	$AceStyr_{15}OPS$	10.6
o-$AceStyr_8OPS$	76.4	$AceStyr_{16}OPS$	74.4
		$AceStyr_{17}OPS$	15.1
Average: 8.1		Average: 16.05	

Complete conversion of the –Br groups is observed in the MALDI-ToF spectra for almost all the compounds, with the exception of $MeStyr_{24}OPS$, which shows small amounts of unreacted –Br groups. This is not completely unexpected, considering the steric hindrance associated with having three –Br groups on a phenyl ring attached to the SQ core, especially for *o*-Br groups.

The MALDI-ToF data of $NBocStyr_xOPS$ show a series of low intensity peaks close to the mass of the deprotected species. We were able to collect MALDI-ToF data for two of the deprotected compounds: *o*-NH_2Styr_8OS and $NH_2Styr_{16}OPS$. No MALDI-ToF data were obtained for $NH_2Styr_{24}OPS$ and $AceStyr_{24}OPS$, most probably due to their complex structures, which makes them unstable under the UV laser of MALDI-ToF such that they fragment. GPC and ceramic yield data for these two compounds (Tables 6 to 8) suggest that nearly all of the –Br groups were converted to the organic derivatives.

Table 6 MALDI-ToF and GPC data for $RStyr_xOPS$

		m/*z* (Ag^+ adduct)		GPC			
R group	x	MALDI[a]	Calc.	M_n	M_w	FW	PDI
Me	8	2068.6	2070.7	1212	1225	1962.8	1.01
	16	2890.4[b]	2983.8	2032	2057	2875.9	1.01
	24	3812	3821.3	2522	2565	3705.2	1.01
NBoc	8	1969.2[b,c]	1971.7[b,c]	2382	2431	2771.6	1.02
	16	3013.9[c]	3015.7[c]	3749	3809	4509.7	1.02
	24	N A	3845.1[c]	4290	4390	6030.6	1.02
Ace	8	2422.2	2422.7	1535	1570	2314.9	1.02
	16	3702.7	3704.1	2542	2614	3596.2	1.03
	24	N A	4877.6	3593	3893	4717.4	1.08

[a] Highest intensity peak detected. [b] As H^+ adduct. [c] As deprotected species (NH_2Styr_xOPS).

Table 7 TGA data for $MeStyr_xOS$ and $AceStyr_xOS$

		Ceramic yield (%)			
R group	x	Actual	Calc.	Calc. with ave FW[a]	$T_{d5\%}$ (°C)
Me	8	24.6	24.5	24.6	367
	16	17.2	16.6	16.8	417
	24	13.5	13	12.9	386
Ace	8	20.3	20.8	21.1	397
	16	13	13.4	13.3	359
	24	5.7	10.2	N.A.	344

[a] Average FW calculated from MALDI-ToF data (Table 3).

Table 8 TGA data for $NBocStyr_xOPS$

	Ceramic yield (%)				Boc group mass (%)	
x	Actual	Calc.	Calc. with ave FW[a]	$T_{d5\%}$ (°C)	Actual	Calc.
8	15.4	17.3	17.2	177/~400	29	29.2
16	11.5	10.2	10.2	190/~440	35	35.9
24	7	8	N.A.	184/~450	38	38.6

[a] Average FW calculated from MALDI-ToF data (Table 2).

GPC analyses of $RStyr_xOPS$ (Table 6) show that these materials exhibit narrow molecular weight distributions, indicating that they retain their silica core structures following reaction. As expected, the methyl derivatives show the lowest molecular weights due to their simple structures. Within each set of functional groups, the molecular weight increases as the number of functional groups per molecule increases. The values of M_n and M_w, as measured by GPC, are smaller than those measured by MALDI-TOF, but expected from GPC characterization of rigid, spherical molecules using flexible, linear standards, based on previous results.[10–12]

TGA data for Me- and $AceStyr_xOPS$, Fig. 4, show mass-loss onset temperatures greater than 350 °C. Table 7 details the actual and theoretical ceramic yields for Me- and $AceStyr_xOPS$. We have also included theoretical ceramic yields calculated using

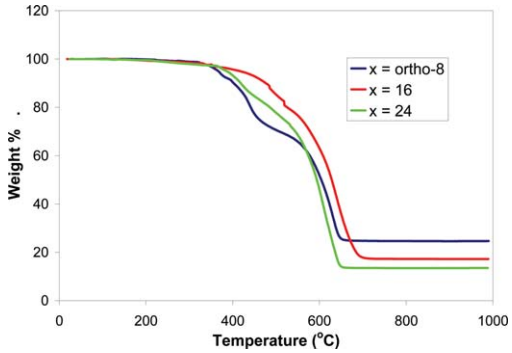

Fig. 4 TGA data in air (10 °C min^{-1}) for MeStyr$_x$OPS (top) and AceStyr$_x$OPS (bottom).

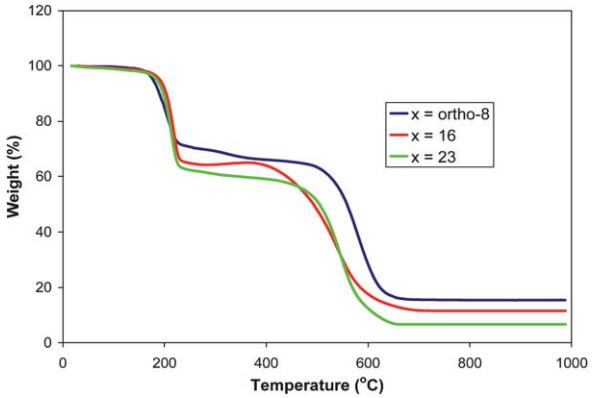

Fig. 5 TGA data in air (10 °C min^{-1}) for NBocStyr$_x$OPS.

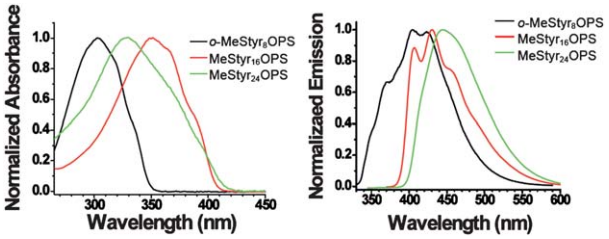

Fig. 6 Absorption and emission spectra for MeStyr$_x$OPS.

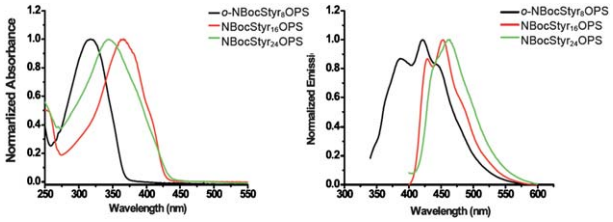

Fig. 7 Absorption and emission spectra for NBocStyr$_x$OPS.

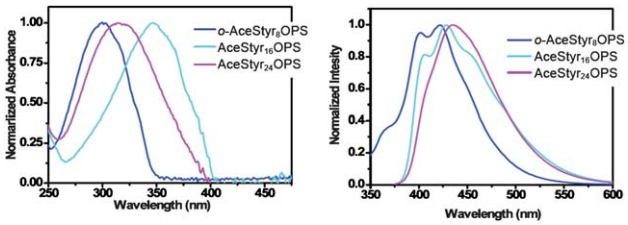

Fig. 8 Absorption and emission spectra for AceStyr$_x$OS.

average FW from MALDI-ToF data. With the exception of AceStyr$_{23}$OPS, the actual and theoretical values of Me- and AceStyr$_x$OPS are in close agreement with each other, confirming that the compositions of the compounds are in accord with the MALDI-ToF data.

TGA data for NBocStyr$_x$OPS (Fig. 5) has two distinct mass loss steps: The first step at ~200 °C arises from the loss of the –Boc protecting group, while the second step at ~400 °C points to the oxidative decomposition of the phenyl groups generating silica as the final ceramic product. Table 8 summarizes the thermal decomposition data of NBocStyr$_x$OPS. The mass loss from the –NBoc groups can be used to estimate the average number of these functional groups per SQ molecule.

Since the actual and theoretical mass loss from the –NBoc groups are comparable, we can assume that all of the –Br groups are converted to the –NBocStyrene groups, in agreement with the MALDI-ToF data.

Photophysical properties

The UV-Vis absorption and photoluminescence spectra for RStyr$_x$OPS are shown in Fig. 6–8. The photophysical data is summarized in Table 9. Within each series of compounds with the same R group, we observed the same trends as discussed below. While consistent in their trends, there are still some important surprises.

First, the absorption and emission spectra for RStyr$_{16}$OPS are red-shifted from those for *o*-RStyr$_8$OPS as expected because of the longer conjugation length. However, the absorption spectra for RStyr$_{24}$OPS are blue-shifted from those for RStyr$_{16}$OPS, whereas the emission spectra are red-shifted. Furthermore, for RStyr$_8$OPS Φ_{PL} are typical of those seen previously at *ca.* 0.04 whereas for the RStyr$_{16}$OPS Φ_{PL} are an order of magnitude higher at 0.40–0.60. Unexpectedly the Φ_{PL} for RStyr$_{24}$OPS are 0.10–0.30 lower than RStyr$_{16}$OPS. This is surprising because it might be anticipated that RStyr$_{24}$OPS would exhibit more extensive conjugation resulting in red-shifts in both the absorption and emission spectra relative to those of RStyr$_{16}$OPS. This should lead to more stabilization in the excited state leading to higher Φ_{PL} values.

In order to explain these results we must first compare the observed behavior with their organic analogs.[27–29] The comparative data are also provided in Table 9. Thus, the absorption spectrum of *o*-MeStyr$_8$OPS has the same λ_{max} as *p*-methylstilbene (Table 9). This is ≈ 20 nm blue-shifted from the absorption λ_{max} of *p*-MeStyr$_8$OPS synthesized from *p*-I$_8$OPS.[11] In contrast, the emission λ_{max} for *p*-methylstilbene is 355 nm compared to 400 nm and 420 nm for *p*-MeStyr$_8$OPS and 405 nm for *o*-MeStyr$_8$OPS.

A comparison of 1,4-distryenylbenzene with MeStyr$_{16}$OPS shows similar absorption λ_{max} of 353 nm and 349 nm, respectively, suggesting similar ground states. The emitting λ_{max} are 408 nm *vs.* 431 nm, which may be accounted for in part by the

Table 9 Photophysical data for $RStyr_xOPS$ (THF, CH_2Cl_2 peak positions are identical)

R group	x	Abs. λ_{max} (nm)	Emis. λ_{max} (nm)	Φ_{PL} %	$\Delta\nu$ Stoke's shift (cm^{-1})	δ GM	δ/group GM
p-MeStilbene[25]		298, 311	355	9			
1,4-Distyrylbenzene[26]		353	385, 408	62			
1,2,4-Tristyrenylbenzene[27]		320, 355[b]					
1,3,5-Tristyrenylbenzene[28]		297	412 (toluene) 384 (hexane)				
p-$MeStyr_8$ OPS[a]		320	400, 422	4			
Me	*o*-8	303	405	4	8312[c]		
	16	349	407, 431, 457	57	5451[c]		
	24	329	444	39	7873[c]		
NBoc	*o*-8	317	386, 422, 445[b]	5	7849[c]	1	~0
	16	364	429, 453	43	5398[c]	50	~3
	24	346	440,[b]461	8	7210[c]	270	~12
Acetoxy	*o*-8	300	402, 422	4	9637[c]	~0	~0
	16	347	407, 429, 451	45	5508[c]	~1	~0
	24	317	435, 453[b]	19	8557[c]	221	~10

[a] *p*-$MeStyr_8OPS$ synthesized from *p*-I_8OPS.[12] [b] Shoulder. [c] There are several emission bands; the emission maximum (underlined) is used to calculate the Stoke's shift.

methyl substituent. In addition, the Φ_{PL} values are quite similar at 62% and 57% (ethanol *vs.* THF).

Finally, comparing 1,2,4-tristyrenylbenzene, 1,3,5-tristyrenylbenzene and $MeStyr_{24}OPS$, we see that the all *meta* 1,3,5-tristyrenylbenzene has an absorption λ_{max} at ≈ 300 nm whereas the 1,2,4-isomer has an absorption λ_{max} at ≈ 320 nm. The emission λ_{max} for the 1,2,4-isomer is not reported but that for the 1,3,5-isomer is 412 nm in toluene. The data suggest that the absorption and emission max for $MeStyr_{24}OPS$ are quite red-shifted from the 1,3,5-tristyrenylbenzene analog but may be similar to or red-shifted from the 1,2,4-isomer as well. Thus, the blue shift for $MeStyr_{24}OPS$ seems explainable in terms of the organic analogs. However, the Φ_{PL} values remain difficult to explain.

Multiple theoretical calculations suggest that the cage is highly electrophilic,[30] which is supported by the fact that it auto-catalyzes bromination as discussed in the accompanying paper.[18] Further support for this comes from our recent studies offering considerable evidence for charge transfer transitions in the excited state leading, for example, to quite high two photon absorption cross sections as discussed below.[10,11] As also noted in the accompanying paper, the cage interacts with aromatic ring substituents as if it were a electron withdrawing substituent equivalent to a CF_3 or NO_2 group.[31]

Consequently, one might expect to see such an electron withdrawing effect on the stilbene substituents prepared here ($RStyr_8OPS$) whether they are *ortho*- or *para*-substituents. The implication is that the cages should cause considerable blue shifts in both the absorption and emission maxima. This is contrary to what is seen. Therefore this argument cannot be used to explain the blue shift in the absorption data for the *ortho*-stilbene (*o*-$MeStyr_8OPS$). The only other possible explanation that seems valid is that the styrenyl group in the *ortho* position is forced to spend some of its time above the cage face. The crystal structure of the starting [*o*-$BrPhSiO_{1.5}$] indicates that the bromo group sits over the face of the very electrophilic cage.[18] Indeed, this interaction might actually be stabilized if the cage is considered to be highly electrophilic. In fact, Bowers *et al.* calculate that the highly electrophilic behavior extends beyond the cage,[30] supporting the suggestion that the cage face polarizes Br_2, promoting *ortho*-substitution, and the possibility that the styrenyl group prefers to sit above the electrophilic cage face.[18] This latter interaction could explain the blue shift relative to the *para* analog (*p*-$MeStyr_8OPS$).

However, the emission spectrum of *o*-$MeStyr_8OPS$ is clearly red-shifted from that of *p*-methylstilbene and similar to that of *p*-$MeStyr_8OPS$. The quantum yield of *o*-$MeStyr_8OPS$ is also similar to *p*-$MeStyr_8OPS$. In our previous work, we attributed the red-shifts in the absorption and emission spectra of *p*-$MeStyr_8OPS$ compared to molecular stilbene to 3-D conjugation as involving the LUMO of the SQ cage.[11] It appears that the excited states of both *o*- and *p*-$MeStyr_8OPS$ are quite similar allowing for the argument that both excited states access the same LUMO inside the SQ cage.

The absorption and emission spectra of $NBocStyr_xOPS$ are only slightly red-shifted from those of $MeStyr_xOPS$ and $AceStyr_xOPS$. This is expected given that the amino groups are masked by the Boc protecting groups, which are electron withdrawing. We would expect much larger red-shifts from free amino groups due to their strong donor characteristics, as seen previously.[10,11] Normally, *para*-alkoxy substituents exhibit good-to-excellent electron donating properties; however, the $AceStyr_xOS$ absorption and emission spectra are similar to $MeStyr_xOS$ suggesting roughly equivalent electron-donating abilities. Thus the electron-withdrawing characteristics of the acyl group seems to balance the normal electron donating properties of a *para* oxygen substituent, but the TPA data suggest this is not quite a correct assessment (see below).

The absorption and emission spectra of $RStyr_{16}OPS$ are both red-shifted from those of *o*-$RStyr_8OPS$ as expected considering the longer conjugation lengths. The absorption maxima and quantum yields for $RStyr_{16}OPS$ are comparable to those for the small molecule analog, 1,4-distyrylbenzene, while the emission spectra are red-shifted from 1,4-distyrylbenzene (20–45 nm

depending on the R-group). The emission spectra of $RStyr_{16}OPS$ exhibit structured bands typical for conjugated aromatic compounds. These compounds also have low two-photon cross-sections (GM values, see Table 9). All of these observations, as briefly noted above, suggest that the HOMO and LUMO of $RStyr_{16}OS$ are similar to those of 1,4-distyrylbenzene without any contributions from the SQ cage.[28] The simplest explanation for this behavior is that the presence of the second styrenyl group on each corner of the cage causes overcrowding around the cage, forcing the distyrenylphenyl groups away from the cage face. It also may interrupt the 3-D interaction with the cage in the excited state. Thus we observe photophysical behavior expected for an electronically isolated organic fragment. This contrasts with the $RStyr_{24}OPS$ compounds.

The blue-shifts in the $RStyr_{24}OPS$ absorption spectra compared to those of $RStyr_{16}OPS$ likely arise from the *meta*-styrenyl groups present on each central phenyl ring (see Fig. 9). As discussed in the accompanying paper on the polybromination of OPS,[18] Br substitution starts at the *ortho*-position (position 1 in Fig. 9). The second Br- adds (almost exclusively) *para*- to the first Br- (position 5 in Fig. 9). We believe that at this point, the steric hindrance will prevent addition of a third Br to the other *ortho*-position (position 6, Fig. 9). Therefore, addition of a third Br would be expected to occur at either of the two other positions on the phenyl rings (positions 3 and 4 in Fig. 9), as supported by the X-ray single crystal data from the accompanying paper, which shows partial occupancy at both positions. This means that there will always be two styrenyl groups *meta* to each other in $RStyr_{24}OPS$.

Previous work on 1,2,4-tristyrylbenzene[28] suggests that its absorption spectrum can be considered as a summation of the 1,3-distyrylbenzene and 1,4-distyrylbenzene spectra, with a maximum (320 nm) in between the maxima of the two distyrylbenzenes (300 nm and 355 nm) and a shoulder corresponding to the absorption maximum of 1,4-distyrylbenzene (355 nm). The authors attribute this phenomenon to interactions between the two conjugated distyrylbenzene "fragments" of the molecule. However, no rationalization as to what these interactions might be is available in the literature.

Related work suggests that *meta*-substituted phenylenevinylene units in *meta*-distyrylbenzene and oligo(phenylenevinylene) can be considered "conjugative insulators" that disrupt the interaction between phenylenevinylene units.[28,29] The 1,3,5-tristyrylbenzene absorption λ_{max}, where all phenylenevinylene units are *meta*-, is 297 nm (toluene or n-hexane) and the emission λ_{max} at 412 nm in toluene.[29]

In comparison, we begin by considering the widths of the absorption bands for $RStyr_{24}OPS$. For each series of R-groups, the absorption spectrum of $RStyr_{24}OPS$ has an onset similar to

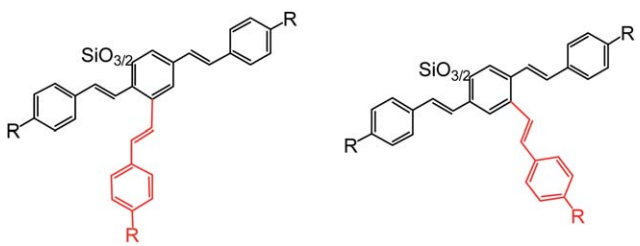

Fig. 9 Two possible configurations of $RStilbene_{24}OS$ corner.

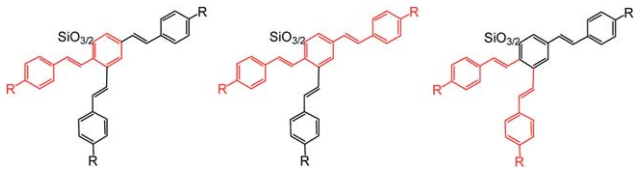

Fig. 10 Interactions of "fragments" of tristyrenylphenyl groups on each corner of $RStyr_{24}OS$.

that for *o*-$RStyr_8OPS$ that tails into the absorption spectrum for $RStyr_{16}OPS$. Each has a λ_{max} in between the maxima of *o*-$RStyr_8OPS$ and $RStyr_{16}OPS$. This implies that the absorption spectra for each $RStyr_{24}OPS$ actually consist of contributions from all "fragments" of the tristyrenylphenyl groups. Basically we observe a sum of the interaction between the *ortho*-stilbenes with the face of the SQ cage (Fig. 10a) with the longer conjugation of the distyrylbenzene units (Fig. 10b) coupled with the disruption in overall conjugation caused by the *meta*-positioned styrenyl (a.k.a. phenylenevinylene) units (Fig. 10c). The presence of the third styrenyl group on each corner of the cage causes even more crowding around the cage and some of the organic groups are forced to approach the face of the cage, thus giving rise to an interaction (blue shift) between the cage face and the organic groups observed in the absorption spectra.

The emission spectra for $RStyr_{24}OPS$ are red-shifted from their respective $RStyr_{16}OPS$ and show no band structure. Their quantum yields are slightly lower, but the two-photon cross-section values are much higher for the NBoc and Acetoxy groups, see Table 9 and Fig. 11. The data suggest that there are actually two pathways for the transition from the excited to the ground state: charge transfer (CT) and normal radiative emission from a π^* state.

The CT effects explain the lack of structure in their emission spectra and the two high TPA values (see below). Normally CT funnels energy away from luminescence and gives rise to low quantum yields. However, in the case of $RStilbene_{24}OS$, the Φ_{PL} values are not as low as expected if CT is the only mechanism for excited-to-ground state transition. The normal π^* radiative emission provides another option, and explains the Φ_{PL} values of $RSyr_{24}OS$. For both mechanisms to be active, both processes must have roughly equivalent decay rates and energies, otherwise one would dominate over the other. Indeed, this suggests that one might promote the CT transition by using a more polar solvent to stabilize the CT transition state and perhaps improve the TPA values at the expense of the Φ_{PL} values. Such studies are planned in the future.

One final comment about these results should be made. Because of the very high density of functional groups, it is possible that some form of 3-D through space interactions are also involved in their absorption and emission behavior. At this point, we have no proof but believe the possibility should be mentioned as higher densities of functional groups affect absorption and emission behavior in cyclic polystyrenes albeit mostly causing blue shifts.[32]

As mentioned above, efforts to deprotect $NBocStyr_xOPS$ to give NH_2Styr_xOPS for MALDI-ToF samples led to rapid oxidation of the amino groups because of the aqueous acidic reaction conditions. Attempts to deprotect the NBoc groups using trifluoroacetic acid were also not successful. Our

previous work with hexadecaaminophenylsilsesquioxane, $[(NH_2)_2PhSiO_{1.5}]_8$, shows it to be very basic and very susceptible to air oxidation at room temperature.[33] Thus, we were concerned that similar efforts to generate samples for photophysical studies would risk including contributions from oxidized materials. Therefore, we decided that it was best to assess the photophysical properties of the NBocStyr$_x$OPS and AceStyr$_x$OPS as discussed below.

Two-photon excited fluorescence measurements

The interaction of the functional groups at the corners of the cage can be very strong and it has been shown previously that this interaction can lead to new optical properties.[11] The possibility of enhancement of the cage macromolecule's two-photon absorption cross-section may result in possible applications in not only optical limiting and sensor protection but the enhanced transition moment of these systems may also lead to enhanced solar energy harvesting devices. In this section we discuss the linear and nonlinear optical properties of this new class of SQs and probe their two-photon absorption properties both in magnitude and spectral width.

Table 9 provides much of the data taken in the current studies. The steady state absorption and emission spectra shown in Fig. 6–8 are displayed comprehensively in Figure S7. As noted above, our efforts were directed towards understanding the photophysical effects of increasing functional group density in the same volume. Our previous studies provide a baseline for the studies conducted here.[10,11] In addition to the steady state studies summarized in the Table 9 data, we also carried out TPA measurements to investigate the charge transfer character.

Two-photon excited-state fluorescence (TPEF) measurements with a femtosecond laser were used to measure TPA cross-sections as a function of wavelength. It is clear from Fig. 11 that the NBocStyr$_x$OPS compounds offer superior TPA cross-sections when compared with the AceStyr$_x$OPS compounds for RStyr$_{16}$OPS and RStyr$_{24}$OPS. This can be explained by the greater strength of the donor group and by changes in the dipole-moment.[34,35] It was also noted that TPA cross sections increase with an increase in the number of chromophores attached to the phenyl group. As seen in Table 9, the cross-sections "per chromophore" in RStyr$_{24}$OPS are also enhanced by the additional chromophores in comparison with RStyr$_{16}$OPS and *o*-RStyr$_8$OPS systems.

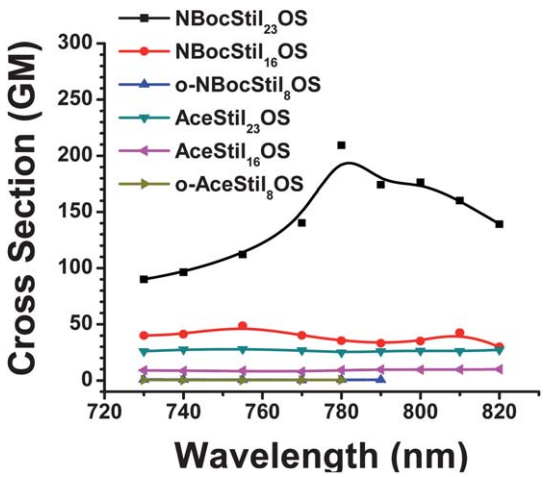

Fig. 11 TPA cross section measurements of the investigated chromophores.

For NBocStyr$_{24}$OPS and NBocStyr$_{16}$OPS, the cross-section increases by a factor of 4.4, while the cross-section increase per chromophore is by a factor of 3. This seems to correlate well with the increase of the cross-section per chromophore, which seems to correlate well with the steady-state measurements of Table 9. In the case of RStyr$_{16}$OPS, although the absorption measurements showed a red shift, the fluorescence emissions and quantum yields suggest that the system possesses less charge transfer character. The literature suggests that molecular systems with symmetric charge transfer from the ends of a conjugation to the middle gives enhanced TPAs,[36] such as found here for RStyr$_{16}$OPS and RStyr$_{24}$OPS. Similar trends are observed in AceStyr$_x$OPS systems as well. Note that *o*-NBocStyr$_8$OPS and *o*-AceStyr$_8$OPS with cross-sections below 1 GM, do not appear to be promising two photon materials, but it may be that on deprotection they will offer TPAs equivalent to the *para* systems we have studied before.[8] Finally, time-resolved measurements are underway in order to understand the actual mechanism of the charge transfer character of these systems.[37]

Conclusions

A series of stilbene-SQs (RStyr$_x$OPS, x = 8, 16, 24; *R* = 4-methylstyrenyl, 4-acetoxystyrenyl, Boc-protected 4-aminostyrenyl) have been synthesized from the corresponding bromophenyl-SQs, $[o\text{-}BrPhSiO_{1.5}]_8$, $[2,5\text{-}Br_2PhSiO_{1.5}]_8$, and $[Br_3PhSiO_{1.5}]_8$. These molecules have some of the highest densities of functional groups/unit volume of any molecules even when compared to silsesquioxane dendrimers.[3–12,38–40] The blue shift in the absorption spectra and red shift in the emission spectra of *o*-RStyr$_8$OPS compared to the small molecule analog suggests interactions between the electrophilic face of the SQ cage with the *ortho*-positioned organic group. In contrast, RStyr$_{16}$OPS exhibit absorption and emission spectra as well as quantum efficiencies typical of simple organic compounds, most likely because of steric interaction forcing the organic groups away from the cage and disrupts the 3-D conjugation involving LUMO inside the SQ cage. RStyr$_{24}$OPS exhibits photophysical behavior that shows characteristics of both regular π–π^* transition and charge transfer, suggesting that there are two excited states of nearly equivalent energy with similar decay rates, involving the LUMO inside the SQ cage as charge acceptor site. We expect these compounds to offer much greater TPA properties if suitable alternative methods of protecting the free amine from oxidation or replacing the acetoxy group are found (*e.g.* with perhaps using alkyl or aryl groups).

Acknowledgements

We would like to thank NSF for funds through grant CGE 0740108 with early work being funded by NSF IGERT Grant DGE-9972776. Early work was also supported in part by Canon Ltd and Mayaterials Inc. Most recently our work on the

photophysical and spectroscopic analysis of the title compounds was supported by a DOE Center Grant Award No. DE-SC0000957.

Notes and references

1 (*a*) P. D. Lickiss and F. Rataboul, *Adv. Organomet. Chem.*, 2008, **57**, 1; (*b*) D. B. Cordes, P. D. Lickiss and F. Rataboul, *Chem. Rev.*, 2010, **10**, 2081.
2 R. M. Laine and M. F. Roll, *Macromolecules*, 2011, **44**, 1073.
3 K. L. Chan, P. Sonar and A. Sellinger, *J. Mater. Chem.*, 2009, **19**, 9103.
4 W.-J. Lin, W.-C. Chen, W.-C. Wu, Y.-H. Niu and A. K.-Y. Jen, *Macromolecules*, 2004, **37**, 2335.
5 J. Lee, H.-J. Cho, B.-J. Jung, N.-S. Cho and H.-K. Shim, *Macromolecules*, 2004, **37**, 8523.
6 S. Xiao, M. Nguyen, X. Gong, Y. Cao, H. Wu, D. Moses and A. J. Heeger, *Adv. Funct. Mater.*, 2003, **13**, 25.
7 C.-H. Chou, S.-L. Hsu, K. Dinakaran, M.-Y. Chiu and K.-H. Wei, *Macromolecules*, 2005, **38**, 745.
8 A. Sellinger, R. Tamaki, R. M. Laine, K. Ueno, H. Tanabe, E. Williams and G. E. Jabbour, *Chem. Commun.*, 2005, 3700.
9 M. Y. Lo, C. Zhen, M. Lauters, G. E. Jabbour and A. Sellinger, *J. Am. Chem. Soc.*, 2007, **129**, 5808.
10 S. Sulaiman, A. Bhaskar, J. Zhang, R. Guda, T. Goodson III and R. M. Laine, *Chem. Mater.*, 2008, **20**, 5563.
11 R. M. Laine, S. Sulaiman, C. Brick, M. Roll, R. Tamaki, M. Z. Asuncion, M. Neurock, J.-S. Filhol, C.-Y. Lee, J. Zhang, T. Goodson III, M. Ronchi, M. Pizzotti, S. C. Rand and Y. Li, *J. Am. Chem. Soc.*, 2010, **132**, 3708.
12 M. Z. Asuncion and R. M. Laine, *J. Am. Chem. Soc.*, 2010, **132**, 3723.
13 T. Yildirim, P. M. Gehring, D. A. Neumann, P. A. Eaton and T. Emrick, *Carbon*, 1998, **36**, 809.
14 J. Lee, C. K. Hong, S. Choe and S. E. Shim, *J. Colloid Interface Sci.*, 2007, **310**, 112.
15 S. Bachmann, H. Wang, K. Albert and R. Partch, *J. Colloid Interface Sci.*, 2007, **309**, 169.
16 S.-G. Kim, S. Sulaiman, D. Fargier, R. M. Laine, in *Materials Syntheses. A Practical Guide*. ed. Schubert, U.; Hüsing, N.; Laine, R. M.; Springer-Verlag, Wein 2008, pp. 179.
17 M. Roll, M. Z. Asuncion, J. Kampf and R. M. Laine, *ACS Nano*, 2008, **2**, 320.
18 M. F. Roll, P. Mathur, K. Takahashi, J. W. Kampf and R. M. Laine, *J. Mater. Chem.*, 2011, DOI: 10.1039/c1jm11536g.
19 M. F. Roll, "*Symmetric Functionalization of Polyhedral Phenylsilsesquioxanes as a Route to Nano-Building Blocks.*" PhD dissertation, University of Michigan, 2010. Molecular diameters were calculated based on single crystal X-ray data for silsesquioxane molecules with similar structures [$Styr_8OPS$ and $(PhC{\equiv}C)_8OPS$] assuming cubic unit cells.
20 B. K. Nanjwade, H. M. Bechra, G. K. Derkar, F. V. Manvi and V. K. Nanjwade, *Eur. J. Pharm. Sci.*, 2009, **38**, 185.
21 A. Maciejewski and R. P. Steer, *J. Photochem.*, 1986, **35**, 59.
22 C. Xu and W. W. Webb, *J. Opt. Soc. Am. B*, 1996, **13**, 481.
23 C. Brick, R. Tamaki, S.-G. Kim, M. Asuncion, M. Roll, T. Nemoto and R. M. Laine, *Macromolecules*, 2005, **38**, 4655.
24 C. E. Garrett and K. Prasad, *Adv. Synth. Catal.*, 2004, **346**, 889.
25 S. E. Letant, J. Herberg, L. N. Dinh, R. S. Maxwell, R. L. Simpson and A. P. Saab, *Catal. Commun.*, 2007, **8**, 2137.
26 L. G. Samsonova, T. N. Kopylova, N. N. Svetlichnaya and O. S. Andrienko, *High Energy Chem.*, 2002, **36**, 276.
27 H. Meier, *Angew. Chem., Int. Ed. Engl.*, 1992, **31**, 1399.
28 L. Ya. Malkes and T. P. Boronenko, *Zhurnal Prikladnoi Spektroskopii*, 1974, **21**, 172.
29 H. Meier, R. Zertani, K. Noller, D. Oelkrug and G. Krabichler, *Chem. Ber.*, 1986, **119**, 1716.
30 See for example: S. E. Anderson, D. J. Bodzin, T. S. Haddad, J. A. Boatz, J. M. Mabry, C. Mitchell and M. T. Bowers, *Chem. Mater.*, 2008, **20**, 4299.
31 F. J. Feher and T. A. Budzichowski, *J. Organomet. Chem.*, 1989, **379**, 33.
32 T. E. Hogen-Esch, *J. Polym. Sci., Part A: Polym. Chem.*, 2006, **44**, 2139.
33 K. Takahashi, S. Sulaiman, J. M. Katzenstein, S. Snoblen and R. M. Laine, *Aust. J. Chem.*, 2006, **59**, 564.
34 G. Ramakrishna, A. Bhaskar and T. Goodson III, *J. Phys. Chem. B*, 2006, **110**, 20872.
35 G. Ramakrishna and T. Goodson III, *J. Phys. Chem. A*, 2007, **111**, 993.
36 M. Albota, D. Beljonne, J.-L. Bredas, J. E. Ehrlich, J. Y. Fu, A. A. Heikai, S. E. Hess, T. Kogej, M. D. Levin, S. R. Marder, D. M. Maughon, J. W. Perry, H. Rockel, M. Rumi, G. Subramaniam, W. W. Webb, X.-L. Wu and C. Xu, *Science*, 1998, **281**, 1653.
37 J. Zhang, T. Goodson III, unpublished work.
38 B. Hong, T. P. S. Thoms, H. J. Murfee and H. J. Lebrun, *Inorg. Chem.*, 1997, **36**, 6146.
39 F. J. Feher and K. D. Wyndham, *Chem. Commun.*, 1998, 323.
40 P. R. Dvornic, C. Hartmann-Thompson, S. E. Keinath and E. J. Hill, *Macromolecules*, 2004, **37**, 7818.